

Synchronous Position Control Strategy for Bi-cylinder Electro-pneumatic Systems

Hong Zhao and Pinhas Ben-Tzvi



International Journal of Control, Automation and Systems 14(6) (2016)
1501-1510

ISSN:1598-6446 (print version)
eISSN:2005-4092 (electronic version)

To link to this article:

<http://dx.doi.org/10.1007/s12555-014-0506-5>

Synchronous Position Control Strategy for Bi-cylinder Electro-pneumatic Systems

Hong Zhao and Pinhas Ben-Tzvi*

Abstract: Pneumatic systems have been widely used in industrial applications because of their well-known advantages. However, pneumatic systems possess several disadvantages that include strong non-linearity and low natural frequency. These drawbacks make it difficult to obtain satisfactory control performances in comparison to hydraulic and electromechanical systems. In this paper, the fundamental characteristics and nonlinear synchronous control strategy of pneumatic systems are studied. A two-layer sliding mode synchro-system based on friction compensation is applied to electro-pneumatic cylinders and a synchro-PID controller is utilized for position tracking. To validate the developed strategy, experiments with bi-cylinder electro-pneumatic systems were performed. The experimental results demonstrate that the synchronous position control scheme is effective in terms of accuracy and robustness.

Keywords: Friction compensation, pneumatic servo system, sliding mode control, synchro-PID controller.

1. INTRODUCTION

With the development of aerospace technologies and modern machine manufacturing, pneumatic actuators have been widely used in numerous engineering areas. The advantages of pneumatic actuators include clean operation and easy serviceability. In most cases, their application is limited to point to point control. The disadvantages of the pneumatic system mainly include air compressibility, strong non-linearity and large mechanical friction. These drawbacks restrict their applications in servo-controlled systems.

More effort has been dedicated to improving this research field. Numerous researchers focused their efforts on studying different aspects of pneumatic servo systems, such as air flow, thermodynamics, linear and non-linear dynamics, valve modelling and friction modelling [1, 2]. Due to high friction in pneumatic systems [3], disturbances lead to system uncertainties. This is usually considered to be the main problem in pneumatic control.

In recent years, the development of pneumatic systems and the improvement of control theories has led to the implementation of modern control laws in pneumatic devices [4–11]. Sliding mode control has been used as a robust nonlinear control technique in many applications requiring insensitivity to parametric uncertainty [12–14].

Over the last decade, multi-surface sliding mode control received a lot of attention [15–19], mainly due to the advantages this tool presents, from higher accuracy and the possibility of using continuous control laws, to the possibility of utilizing the Coulomb friction model in control algorithms [20] and the finite time convergence for systems with arbitrary relative degrees [21].

However, new requirements in the performance of pneumatic systems are continually being proposed. The need for motion synchronization between multiple pneumatic actuators for lifting and rolling applications has been the focus of the research efforts [22, 23].

In order to eliminate the synchro error and improve the control performance with one air source - especially reducing the effects of static friction - a bi-cylinder controller design is proposed. In this paper, the electro-pneumatic motion synchronization servo control system with one air source is introduced, and the fundamental characteristics and the nonlinear control strategy of the pneumatic system are studied. A bi-cylinder controller is adopted for the control of the electro-pneumatic synchro position system, and the effectiveness of the proposed technique is demonstrated through simulations and experiments.

Manuscript received November 16, 2014; revised June 28, 2015 and November 3, 2015; accepted December 27, 2015. Recommended by Associate Editor Won-jong Kim under the direction of Editor Hyouk Ryeol Choi. This work was in part supported by the National Natural Science Foundation of China (Grant No. 51575528).

Hong Zhao is with the College of Mechanical and Transportation Engineering, China University of Petroleum, Beijing 102249, China (e-mail: hzhao_cn@163.com). Pinhas Ben-Tzvi is with the Department of Mechanical Engineering and the Department of Electrical and Computer Engineering, Virginia Tech, Blacksburg, VA 24061, USA (e-mail: bentzvi@vt.edu).

* Corresponding author.

2. SYSTEM DESCRIPTION

2.1. Configuration of the electro-pneumatic position synchro servo control system

The proposed servo control system consists of two rodless pneumatic cylinders controlled by two proportional directional valves as shown in Figs. 1(a) and (b). The experimental sampling rate is 2.5 KHz. The main components of the system are as follows: Two Festo electro-pneumatic five-port proportional valves: MPYE-5-1/4-010B; maximum flow rate 1400 l/min, operating voltage DC 24 V, voltage variant: 0-10 V, Nominal width 8mm; Two rodless pneumatic cylinders with 600 mm stroke length: DGP-40-600-PPV-A-B; One air source: maximum pressure 0.6 MPa, maximum flow rate 1500 l/min; Four pressure sensors: PT351-0.6MPa-0.3, resolution 0.3%; Two position sensors: MLO-POT-600-TLF, resolution 0.01 mm; Mass load A (5.75 kg) and B (5.85 kg) are mounted on sliding parts, which are connected to the pistons of cylinders A and B, respectively. External forces of 17 N and 34 N are applied to cylinder A to simulate external load disturbances.

2.2. Computer software

The pneumatic control software that we developed for the purpose of this study was the key component in obtaining experimental results. It includes the human-machine interface built in LabWindows/CVI [24], the control algorithm as well as the data processing routines.

3. MATHEMATICAL MODEL

3.1. Subsystem 1 (with cylinder A)

A nonlinear state-space model of the system is derived based on a single cylinder pneumatic model from reference [5], as follows:

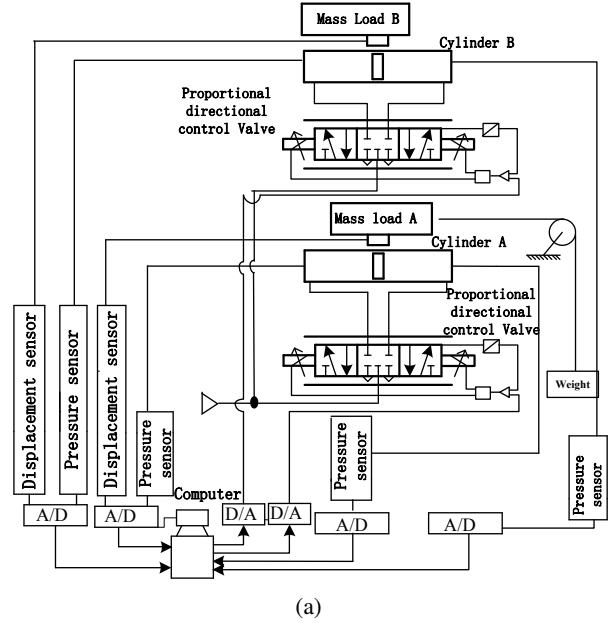
$$\dot{x}_1 = \dot{x} = x_2, \quad (1)$$

$$\dot{x}_2 = \frac{A_p}{M_1} (p_{x1} - p_{x2}) - \frac{F_{f1}}{M_1} - \frac{F_1}{M_1}, \quad (2)$$

$$\begin{aligned} \dot{x}_3 &= \dot{p}_{x1} \\ &= \frac{\frac{kRC_d C_0}{\sqrt{RT}} \left[A_{1s}(u_1) \cdot p_s \cdot f\left(\frac{p_{x1}}{p_s}\right) - A_{1e}(u_1) \cdot p_{x1} \cdot f\left(\frac{p_e}{p_{x1}}\right) \right]}{V_{10} + \frac{1}{2}A_p L + A_p x_1} \\ &\quad - \frac{kA_p p_{x1} x_2}{V_{10} + \frac{1}{2}A_p L + A_p x_1}, \end{aligned} \quad (3)$$

$$\begin{aligned} \dot{x}_4 &= \dot{p}_{x2} \\ &= \frac{\frac{kRC_d C_0}{\sqrt{RT}} \left[A_{2s}(u_1) \cdot p_s \cdot f\left(\frac{p_{x2}}{p_s}\right) - A_{2e}(u_1) \cdot p_{x2} \cdot f\left(\frac{p_e}{p_{x2}}\right) \right]}{V_{20} + \frac{1}{2}A_p L - A_p x_1} \\ &\quad + \frac{kA_p p_{x2} x_2}{V_{20} + \frac{1}{2}A_p L - A_p x_1}. \end{aligned} \quad (4)$$

Definitions for other parameters are provided in the nomenclature.



(a)



(b)

Fig. 1. (a) Scheme of the experimental system, (b) photos of the experimental setup.

3.2. Subsystem 2 (with cylinder B)

$$\dot{z}_1 = \dot{z} = z_2, \quad (5)$$

$$\dot{z}_2 = \frac{A_p}{M_2} (p_{z1} - p_{z2}) - \frac{F_{f2}}{M_2} - \frac{F_2}{M_2}, \quad (6)$$

$$\begin{aligned} \dot{z}_3 &= \dot{p}_{z1} \\ &= \frac{\frac{kRC_d C_0}{\sqrt{RT}} \left[A_{1s}(u_2) \cdot p_s \cdot f\left(\frac{p_{z1}}{p_s}\right) - A_{1e}(u_2) \cdot p_1 \cdot f\left(\frac{p_e}{p_{z1}}\right) \right]}{V_{10} + \frac{1}{2}A_p L + A_p z_1} \\ &\quad - \frac{kA_p p_{z1} z_2}{V_{10} + \frac{1}{2}A_p L + A_p z_1}, \end{aligned} \quad (7)$$

$$\begin{aligned} \dot{z}_4 &= \dot{p}_{z2} \\ &= \frac{\frac{kRC_d C_0}{\sqrt{RT}} \left[A_{2s}(u_2) \cdot p_s \cdot f\left(\frac{p_{z2}}{p_s}\right) - A_{2e}(u_2) \cdot p_{z2} \cdot f\left(\frac{p_e}{p_{z2}}\right) \right]}{V_{20} + \frac{1}{2}A_p L - A_p z_1} \\ &\quad + \frac{kA_p p_{z2} z_2}{V_{20} + \frac{1}{2}A_p L - A_p z_1}, \end{aligned} \quad (8)$$

where,

$$f\left(\frac{p_d}{p_u}\right) = \begin{cases} \sqrt{\frac{2}{k-1} \cdot \left(\frac{k+1}{2}\right)^{k+1} / k - 1} \\ \times \sqrt{\left[\left(\frac{p_d}{p_u}\right)^{2/k} - \left(\frac{p_d}{p_u}\right)^{k+1/k}\right]} \\ \text{if } p_{atm}/p_u \leq (p_d/p_u) \leq C_r \\ 1 \\ \text{if } C_r \leq (p_d/p_u) < 1. \end{cases}$$

A_{1s} , A_{2s} , A_{1e} and A_{2e} are the valve geometric orifice area function, and they are the nonlinear functions of u [1] (u -valve input opening size). Due to the complexity of the equations, the following linear functions are used for approximation:

$$A_{1s}(u_i) = \pi D u_i, \quad (9)$$

$$A_{2s}(u_i) = \pi D \delta = A_f, \quad (10)$$

$$A_{1e}(u_i) = \pi D \delta = A_f, \quad (11)$$

$$A_{2e}(u_i) = \pi D u_i, \quad (12)$$

where, δ is the valve's clearance, A_f is valve's leakage measurement, D is the piston's valve diameter, cylinder A system, $i = 2$ for cylinder B system.

3.3. Friction model of the system

Friction has an accentuated influence on the step or tracking tasks, mainly when the piston velocity is small. From the experimental position step-input response shown in Fig. 2, the dithering effect at the end of the piston stroke is observed.

Friction forces are the main factor that affects the performance of the pneumatic servo system controller. Those forces are mainly generated by contact between the piston seals and the cylinder walls. This nonlinear effect becomes even more dominant at lower sliding velocities. Typically, friction forces in the cylinder include static and dynamic components. Stribeck model [25] is one of the widely used friction models, but for our experimental application, we simplified the switching process between the Coulomb static friction and the Coulomb dynamic friction. The chosen model is shown in Fig. 3.

When $v > 0$,

$$\begin{aligned} F_f &= F_{s1} - k_2 \cdot v & \text{for } v < v_d, \\ F_f &= F_{s1} - F_{d1} + k_1 \cdot v & \text{for } v \geq v_d, \end{aligned} \quad (13)$$

where v_d is the velocity cut-off point. When $v < 0$, the rest can be deduced by analogy. From experimental tests on the pneumatic cylinders, the friction parameters were estimated and summarized in Table 1.

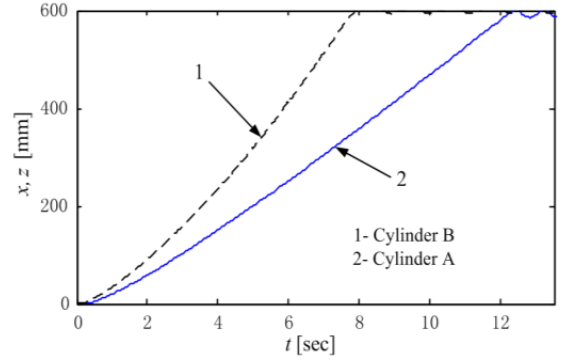


Fig. 2. Open-loop system response to a position step input.

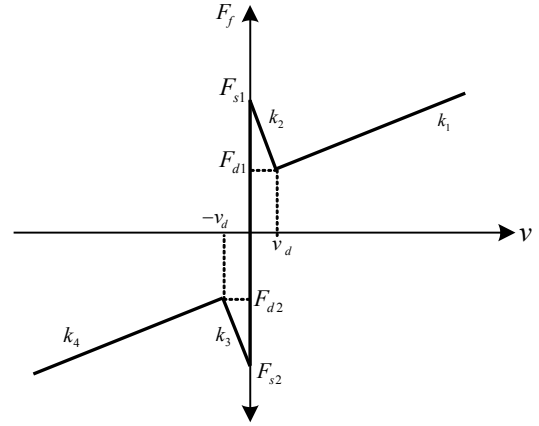


Fig. 3. Simplified friction force model.

Table 1. Friction parameters summary.

Cylinder	k_1	k_4	$F_{d1}(N)$	$F_{d2}(N)$	$F_{s1}(N)$	$F_{s2}(N)$
A	91.83	89.33	54.97	-57.43	84.87	-89.22
B	85.03	86.82	55.06	-63.1	75.52	-75.13

4. CONTROL DESIGN STRATEGY

The block diagram of the proposed controller is shown in Fig. 4. It consists of two cylinder controllers, and a synchro PID controller. Each of the cylinder controllers includes a second order sliding mode controller and a friction compensator. The synchro PID controller coordinates the operation of the two cylinder controllers and improves the synchro motion control of the cylinders. The bi-cylinder synchro controller is required to maintain the displacement error between subsystems 1 and 2 to less than a specified tolerance, keeping their corresponding displacement values to approximately the same. This requirement can be expressed mathematically as follows:

$$\max |x(t) - z(t)| \leq e_t \quad \forall t \in [a, b], \quad (14)$$

where e_t is the permitted position tolerance (it is chosen to eliminate the large error in position tracking), $x(t)$ is

the real position of cylinder A, $z(t)$ is the real position of cylinder B, and $[a, b]$ is the time domain.

Let $e_{sy} = x(t) - z(t)$, $t \in [a, b]$. The synchro PID controller is given by:

$$u_{ad1} = \begin{cases} K_{sy1} |e_{sy}| + K_{sy2} \left| \int e_{sy} dt \right| \\ \quad + K_{sy3} \left| \frac{de_{sy}}{dt} \right|, & e_{sy} < 0 \\ 0, & e_{sy} \geq 0, \end{cases} \quad (15a)$$

$$u_{ad2} = \begin{cases} K_{sy1} e_{sy} + K_{sy2} \int e_{sy} dt \\ \quad + K_{sy3} \frac{de_{sy}}{dt}, & e_{sy} > 0 \\ 0, & e_{sy} \leq 0. \end{cases} \quad (15b)$$

As the synchro PID controllers are made to adjust the difference between two cylinder's displacements, u_{ad1} is added in cylinder A control signal and u_{ad2} is added to cylinder B's control signal. When $e_{sy} = x(t) - z(t) < 0$, cylinder A should be adjusted to keep up with cylinder B's displacement and u_{ad1} should be positive and u_{ad2} is zero. When $e_{sy} = x(t) - z(t) > 0$, cylinder B should be adjusted to keep up with cylinder A's displacement and u_{ad2} should be positive and u_{ad1} is zero.

In order to adjust the parameters of the synchro PID controller, the integral absolute error (IAE) performance minimization measure is considered. The synchro PID controller's parameters are set as follows: $K_{sy1} = 2$, $K_{sy2} = 0.0015$, $K_{sy3} = 0.001$. Based on the mathematical model presented in the previous section, it is clear that pressure functions in the pneumatic cylinder are nonlinear; hence the pressure drop is taken as the sliding mode layers. The bi-layer sliding mode control strategy with friction compensation is proposed in order to overcome friction disturbances in the cylinders. Inner pressure loop control enhances the speed of the system response and attenuates fluctuations in the pressure, hence improving the system tracking accuracy. The control approach is developed as follows.

4.1. Control rule in cylinder A

For the purpose of controller design, if the nonlinear pneumatic model is rewritten in the affine function form with (1)-(4), we can get

$$\begin{cases} \dot{x}_1 = x_2 \\ \dot{x}_2 = \frac{\Delta p \cdot A_p - K_{f1} x_2}{M_1} - \frac{F_{kc} \text{sgn}(x_2)}{M_1} \\ \Delta \dot{p} = (\dot{p}_{x1} - \dot{p}_{x2}) = f_1(x) + g_1(x) \cdot u, \end{cases} \quad (16a)$$

From (16a),

$$\dot{\mathbf{x}} = \mathbf{A}_1 \mathbf{x} + \mathbf{B}_1 \mathbf{p} + \mathbf{q}, \quad (16b)$$

$$\Delta \dot{p} = (\dot{p}_{x1} - \dot{p}_{x2}) = f_1(x) + g_1(x) \cdot u \quad (16c)$$

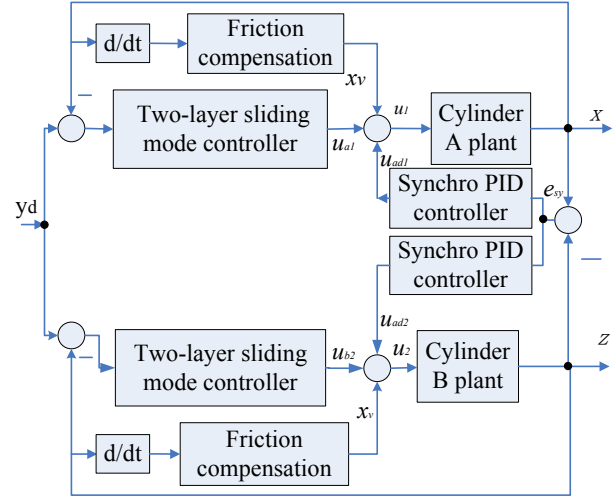


Fig. 4. Block diagram of the integrated control strategy for the bi-cylinder actuator.

$$\text{with } \mathbf{x} = [x_1, x_2]^T, \mathbf{A}_1 = \begin{bmatrix} 0 & 1 \\ 0 & -\frac{K_{f1}}{M_1} \end{bmatrix}, \mathbf{B}_1 = \begin{bmatrix} 0 \\ \frac{A_p}{M_1} \end{bmatrix},$$

$$\mathbf{q} = \begin{bmatrix} 0 \\ -\frac{F_{kc} \text{sgn}(x_2)}{M_1} \end{bmatrix},$$

$$f_1(x) = -\frac{kA_p \dot{x} p_{x1}}{V_{10} + \frac{1}{2} A_p L + A_p x} - \frac{kA_p \dot{x} p_{x2}}{V_{20} + \frac{1}{2} A_p L - A_p x}$$

$$- \frac{kRC_d C_0}{\sqrt{R/T}} \cdot \left(\frac{A_f \cdot p_{x1} \cdot f\left(\frac{p_e}{p_{x1}}\right)}{V_{10} + \frac{1}{2} A_p L + A_p x} + \frac{A_f \cdot p_s \cdot f\left(\frac{p_{x2}}{p_s}\right)}{V_{20} + \frac{1}{2} A_p L - A_p x} \right),$$

$$g_1(x) = \frac{kRC_d C_0 \pi D}{\sqrt{R/T}} \left(\frac{p_s \cdot f\left(\frac{p_{x1}}{p_s}\right)}{V_{10} + \frac{1}{2} A_p L + A_p x} + \frac{p_{x2} \cdot f\left(\frac{p_e}{p_{x2}}\right)}{V_{20} + \frac{1}{2} A_p L - A_p x} \right).$$

It should be noted that the controllability of the plant is proven using (16b) and the controllability matrix.

p_{x1} , p_{x2} cannot be in excess of the range between the supply pressure p_s and the exhaust pressure p_e , therefore the function $f_1(\dots)$ is always positive and g_1^{-1} does exist. The maximum value of g_1^{-1} satisfies $\max |g_1^{-1}| \leq g_m$.

Generally, the static friction force $F_{kc} \text{sgn}(x_2)$ cannot be measured accurately but it is assumed that the maximum value of static friction is known. Since x_d and Δp_d are bounded, \mathbf{q} in (16b) can be treated as a bounded uncertainty.

The simplified diagram for pressure drop is shown in Fig. 5. Let the inner loop tracking error be $e_p = \Delta p - \Delta p_d$

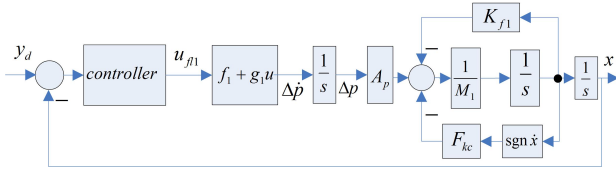


Fig. 5. The block diagram of the single cylinder system with simplified pressure control strategy.

and choose the control input u_{f11} as follows:

$$u_{f11} = \frac{1}{g_1(x)} (-f_1(x) + \Delta \dot{p}_d - k_{ep}(\Delta p - \Delta p_d)). \quad (17)$$

Then we can get

$$\Delta \dot{p} = \Delta \dot{p}_d - k_{ep}(\Delta p - \Delta p_d). \quad (18)$$

A simplified control approach can be adopted by making $\Delta p \rightarrow \Delta p_d$ as $x \rightarrow y_d$. For the inner loop (pressure loop), k is chosen to make the function

$$\dot{e}_p + k_{ep}e_p \rightarrow 0. \quad (19)$$

Then $\Delta p \rightarrow \Delta p_d$.

Let's define the sliding surface by $\sigma = \Delta p - \Delta p_d$. Then:

$$\dot{\sigma}_1 = \Delta \dot{p} - \Delta \dot{p}_d = f_1 + g_1 u - \Delta \dot{p}_d. \quad (20)$$

If the Lyapunov function is chosen to be $V_{lya1} = 0.5\sigma_1^2$, then $\dot{V}_{lya1} = \sigma_1 \dot{\sigma}_1$.

To ensure that $\dot{V}_{lya1} = \sigma_1 \dot{\sigma}_1$ is a negative-definite function, we choose the control law u_s .

When $\sigma_1 < 0$ and $\dot{\sigma}_1 > 0$

$$u_{\sigma_1} > |g_1^{-1} f_1 - g_1^{-1} \Delta \dot{p}_d|. \quad (21)$$

When $\sigma_1 > 0$ and $\dot{\sigma}_1 < 0$

$$u_{\sigma_1} < -|g_1^{-1} (f_1 - \Delta \dot{p}_d)|. \quad (22)$$

However, by the triangle inequality

$$|g_1^{-1} f_1| + |g_1^{-1} \Delta \dot{p}_d| > |g_1^{-1} (f_1 - \Delta \dot{p}_d)|. \quad (23)$$

Then $|g_1^{-1} f_1| + g_m \alpha > |g_1^{-1} (f_1 - \Delta \dot{p}_d)|$.

Therefore, the system can be stabilized by means of control law

$$u_{\sigma_1} = \begin{cases} |g_1^{-1} f_1| + g_m \alpha, & \sigma_1 < 0 \\ -(|g_1^{-1} f_1| + g_m \alpha), & \sigma_1 > 0, \end{cases} \quad (24)$$

and

$$u_{\sigma_1} = -\kappa_1 \text{sgn}(\sigma_1), \quad \kappa_1 > 0, \quad (25)$$

$$\dot{V}_{lya1} = \sigma_1 \dot{\sigma}_1 < 0, \quad (26)$$

and

$$u_{cy1} = u_{f11} - \kappa_1 \text{sgn} \sigma_1. \quad (27)$$

For the outer loop (position loop), Δp_d is chosen to make the function

$$(\ddot{x} - \ddot{y}_d) + \xi_1(\dot{x} - \dot{y}_d) + \xi_2(x - y_d) = 0. \quad (28)$$

The control objective is to obtain the state \mathbf{X} in order to track a desired state $Y_d = (y_d, \dot{y}_d, \ddot{y}_d)$, in the presence of model uncertainties and unknown disturbances.

$$\Delta p = \frac{M_1}{A_p} \ddot{x} + \frac{1}{A_p} (K_{f1} \dot{x} + F_{kc} \text{sgn}(\dot{x})). \quad (29)$$

From (28), we get $\ddot{x} = \ddot{y}_d - \xi_1 \dot{e}_1 - \xi_2 e_1$, where $e_1 = x - y_d$.

The above control law is based on the exact cylinder friction model. This means that there are no other disturbances on the friction factors K_{f1} and F_{kc} . In fact, Δp_d should be modified to improve the robustness of the system. Therefore, a pseudo control input w_1 is added in order to eliminate the changing effects of the friction factors. The expression for Δp_d then becomes

$$\Delta p_d = \frac{M_1}{A_p} [\ddot{y}_d - \xi_1(\dot{x} - \dot{y}_d) - \xi_2(x - y_d)] + \frac{1}{A_p} (\bar{K}_{f1} \dot{x} + \bar{F}_{kc} \text{sgn} \dot{x} + M_1 w_1) + \frac{1}{k} \dot{e}_p, \quad (30)$$

and

$$\Delta p - \Delta p_d = \frac{M_1}{A_p} (\ddot{e}_1 + \xi_1 \dot{e}_1 + \xi_2 e_1) + \frac{1}{A_p} (\Delta K_{f1} \dot{x} + \Delta F_{kc} \text{sgn}(\dot{x}) - M_1 w_1) - \frac{1}{k} \dot{e}_p. \quad (31)$$

External force F_1 is eliminated from equation (31) since this controller is insensitive to external force disturbances.

For $\Delta p \rightarrow \Delta p_d$, equation (31) becomes:

$$\ddot{e}_1 + \xi_1 \dot{e}_1 + \xi_2 e_1 + \frac{1}{M_1} (\Delta K_{f1} \dot{x} + \Delta F_{kc} \text{sgn} \dot{x}) - w_1 = 0, \quad (32)$$

where $\Delta K_{f1} = K_{f1} - \bar{K}_{f1}$ and $\Delta F_{kc} = F_{kc} - \bar{F}_{kc}$ are the friction factors differences, and \bar{K}_f and \bar{F}_{kc} are the exact friction factors.

The second sliding surface is chosen as $e_1 = x - y_d$. Choosing the sliding mode

$$s_1 = \dot{e}_1 + c_1 e_1 = (\dot{x} - \dot{y}_d) + c_1(x - y_d), \quad c_1 > 0, \quad (33)$$

then

$$\begin{aligned} \dot{s}_1 &= \ddot{e}_1 + c_1 \dot{e}_1 = (\ddot{x} - \ddot{y}_d) + c_1(\dot{x} - \dot{y}_d) \\ &= \mathbf{A}_1 \dot{\mathbf{x}} + \mathbf{B}_1 \Delta \dot{p} + \dot{\mathbf{q}} - \ddot{\mathbf{y}}_d - c_1 \dot{\mathbf{x}} - c_1 \dot{\mathbf{y}}_d, \\ \dot{s}_1 &= (\mathbf{A}_1 - c_1 \mathbf{I})(\mathbf{A}_1 \mathbf{x} + \mathbf{B}_1 \Delta p + \mathbf{q}) \\ &\quad + \mathbf{B}_1 (f_1 + g_1 u) + \dot{\mathbf{q}} - \ddot{\mathbf{y}}_d - c_1 \dot{\mathbf{y}}_d. \end{aligned} \quad (34)$$

Let the Lyapunov function be $V_{lya2} = \frac{1}{2}s_1^2$, then

$$\dot{V}_{lya2} = s_1 \dot{s}_1.$$

When $s_1 < 0$ and $\dot{s}_1 > 0$,

$$u_{s1} > \left| \begin{array}{l} B_1^{-1} \cdot g_1^{-1} [(A_1 - c_1 I)(A_1 x + B_1 \Delta p + q) \\ + B_1 f_1 + \dot{q} - \ddot{x}_d - c_1 \dot{x}_d] \end{array} \right|. \quad (35)$$

When $s_1 > 0$ and $\dot{s}_1 < 0$,

$$u_{s1} < \left| \begin{array}{l} B_1^{-1} \cdot g_1^{-1} [(A_1 - c_1 I)(A_1 x + B_1 \Delta p + q) \\ + B_1 f_1 + \dot{q} - \ddot{x}_d - c_1 \dot{x}_d] \end{array} \right|. \quad (36)$$

So

$$u_{s1} = -\varepsilon_1 \operatorname{sgn}(s_1), \quad (37)$$

and

$$\dot{V}_{lya2} = s_1 \dot{s}_1 < 0. \quad (38)$$

Finally, the variable structure control is

$$u_{cy1} = w_1 - \varepsilon_1 \operatorname{sgn}(s_1), \varepsilon_1 > 0. \quad (39)$$

Combining functions (27) and (39) into one control function, the integrated control law becomes

$$u_{a1} = u_{f11} + w_1 - \kappa_1 \operatorname{sgn} \sigma_1 - \varepsilon_1 \operatorname{sgn}(s_1), \quad \kappa_1 > 0, \varepsilon_1 > 0, \quad (40)$$

where K_{f1} is the coefficient of viscous friction; F_{kc} is Coulomb friction in cylinder A; σ_1 and s_1 are the first layer of sliding mode and synthetic sliding mode in cylinder A, respectively.

4.2. Control rule in cylinder B

The second layer of the sliding surface is:

$$s_2 = \dot{e}_2 + c_2 e_2, \quad c_2 > 0. \quad (41)$$

The control rule is:

$$u_{b2} = u_{f12} + w_2 - \kappa_2 \operatorname{sgn} \sigma_2 - \varepsilon_2 \operatorname{sgn}(s_2), \quad \kappa_2 > 0, \varepsilon_2 > 0, \quad (42)$$

where $e_2 = z - y_d$. Parameter definitions in this section are similar to the previous sections for cylinder A with the only difference that subscript 2 in this section pertains to cylinder B.

4.3. Friction compensation

As mentioned in Table 1, the maximum static friction is 89.22 N. When the pressure in the cylinder is below 0.2 MPa, the force is 251.2 N and as such friction cannot be neglected. Therefore, this friction needs to be compensated, and the adopted compensation rule was chosen as follows:

$$x_v = \begin{cases} \Delta_1 & |e| > e_d \text{ and } u_1, u_2 > 0, \\ \Delta_2 & |e| \leq e_d \text{ or } u_1, u_2 = 0, \end{cases} \quad (43)$$

where e_d is the error tolerance; u_1, u_2 are the control value before friction compensation; $\Delta_1 = 0.02, \Delta_2 = 0.04$ are the friction compensation values.

5. EXPERIMENTAL RESULTS

5.1. Fundamental performance analysis of the pneumatic position synchro system

Experiments were conducted to thoroughly study the performance of the pneumatic synchro system control. Experimental results for an open-loop system response to a step input are shown in Figs. 2, 6, 7, and 8.

Fig. 2 shows the displacement response of each piston moving from the initial position (0 [mm]) to the final position of 600 [mm]. The chamber diameter is 40 [mm], and the supply pressure is set to 0.6 [MPa]. Fig. 6 shows the pressure in each cylinder. Fig. 7 shows the displacement of each piston moving from the final to the initial position. Fig. 8 shows the pressure variations in each cylinder.

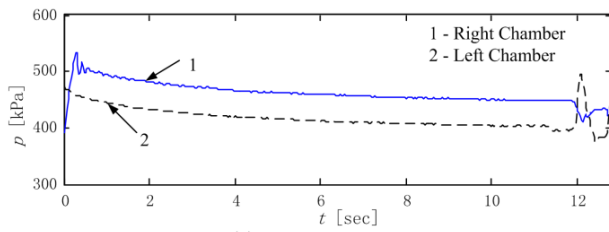
It can be seen from Figs. 2, 6, 7, and 8 that air compressibility introduces time delay in the piston response. Figs. 2 and 7 show that the two cylinders are operating under two different pressures. The cylinder with the lower pressure exhibited more delay in the response and was affected by dithering at the end of the stroke – from 0 [mm] to 600 [mm]. One reason is due to the friction in the cylinders and the other may be attributed to the structure of the cylinder. The inlet and outlet of the rodless pneumatic cylinders are located on the same side. Because air must flow through a long outlet hole in the cylinder, the resistance is relatively larger and hence the flow is not smooth.

According to Fig. 7, when the pistons displace from 600 [mm] to 0 [mm], the outlet hole becomes the inlet hole, and hence pressure dithering is no longer produced. But because the two cylinders operate under one common air source, the pressure in each cylinder is practically not the same. The pressure in cylinder B is lower than that of cylinder A. Therefore, “chattering” is produced in the chamber of cylinder B as shown in Fig. 8(b).

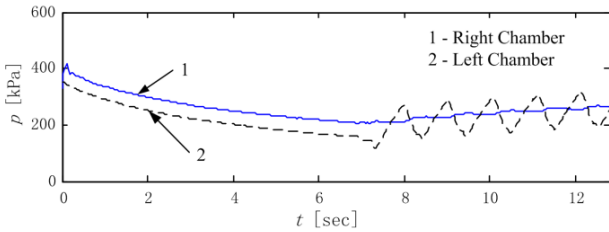
The static friction and dynamic friction in the cylinder and air compressibility made the left chamber in the cylinder show the “chattering” phenomenon, especially in cylinder B. The pressure of the left chamber is low and below a certain value. If the pressure in the left chamber of cylinder B is estimated as 0.15 MPa, the force in the left chamber becomes 188.4 N and the maximum static friction is 75.52 N. The static friction and dynamic friction affect the piston displacement and the pressure in the chamber becomes oscillatory. The load masses, friction, leakage and other effects in both cylinders A and B are not completely identical. In addition, pneumatic systems have the inherent disadvantage of strong nonlinearity and low natural frequency. For all these reasons, it is usually difficult to obtain satisfactory synchro control performances using traditional control methods.

5.2. Performance of PID controller in tracking

Fig. 9 shows the experimental results with an ideal sinusoidal displacement input $y_d(t) = [300 + 100 \sin$



(a) Pressure in Cylinder A.



(b) Pressure in Cylinder B.

Fig. 6. Pressure in cylinders A and B.

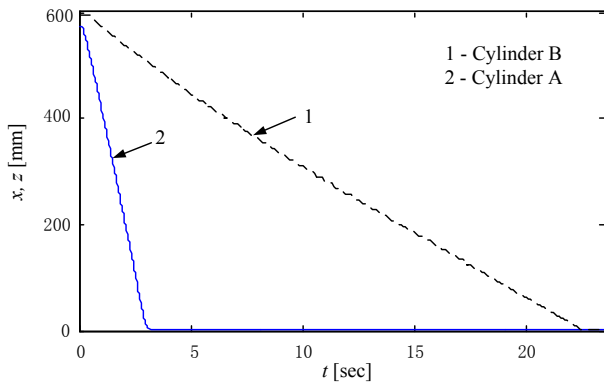


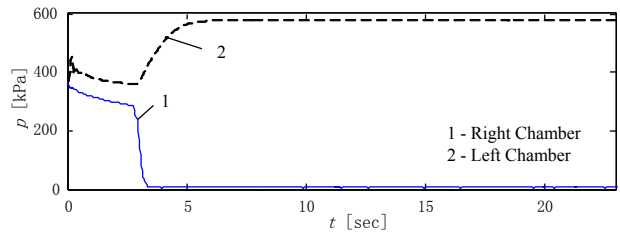
Fig. 7. Open-loop system response to a step input from the other direction.

$(0.314t)$ [mm] and two displacement output responses x, z , for cylinders A and B, respectively. The system is controlled using a classical PID controller with the following control parameters: For cylinder A: $k_p = 6$, $k_i = 0.0015$, $k_d = 0.01$; and for cylinder B; $k_p = 7$, $k_i = 0.004$, $k_d = 0.015$.

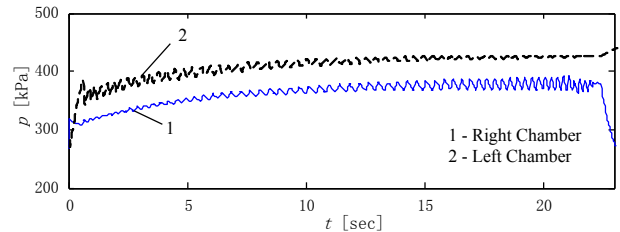
It is clear from Fig. 9 that the response curves are distorted and fail to track the sinusoidal input due to non-linear friction effects. The experimental results show that the displacement synchro relative error between cylinder A and cylinder B is 15%.

5.3. Simulation of the synchronous control strategy

In order to compare the proposed controller with the PID controller, the response simulation is performed. Fig. 10 shows the simulation results with an ideal sinusoidal displacement input $y_d(t) = [0.1 \sin(0.314t)]$ [mm] and two displacement output responses x, z , for cylinders A and



(a) Pressure in Cylinder A.



(b) Pressure in Cylinder B.

Fig. 8. Pressure in cylinders A and B from the other direction.

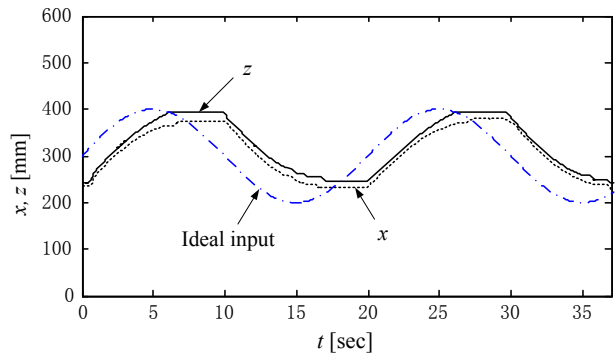


Fig. 9. Tracking synchro control with PID controller.

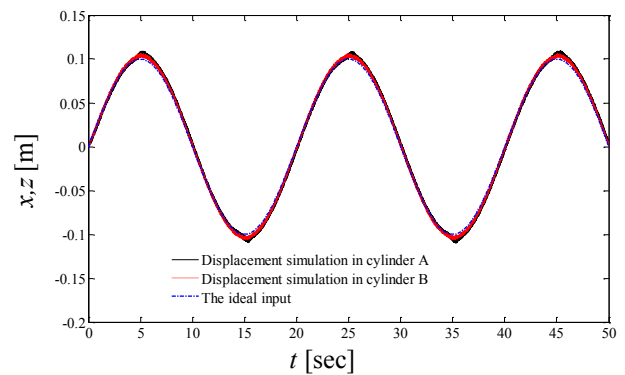


Fig. 10. Tracking synchro control with the proposed controller.

B, respectively. From Fig. 10, the proposed controller shows better performances in synchro-tracking. The sliding mode control signal is shown in Fig. 11 and the total control signal is shown in Fig. 12.

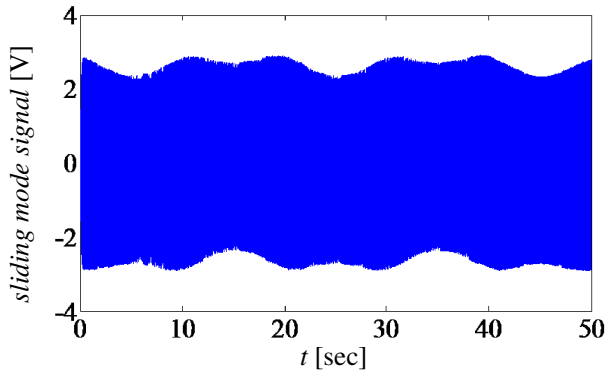


Fig. 11. The proposed sliding model signal.

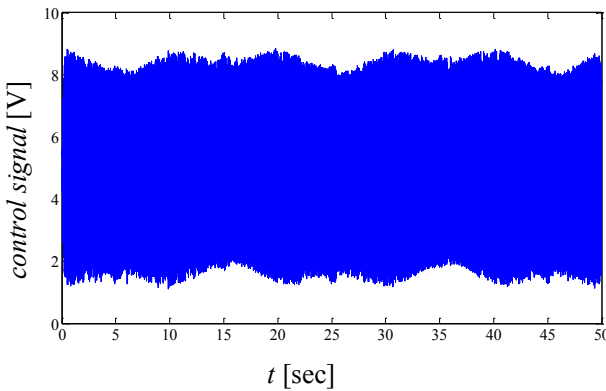


Fig. 12. The proposed control signal.

5.4. Experimental performance of the proposed synchronous control strategy

Fig. 13 shows the experimental results of the displacement output of cylinders A and B performed under different displacement inputs. In this experiment, we used the synchronous control strategy and two-layer sliding mode control with feedback linearization based on friction compensation as proposed earlier. No external load was applied to cylinder A. Fig. 10 shows the step response (with 300 [mm] step size), with maximum relative synchro error of 3%.

Fig. 14 shows the experimental results for the synchro tracking sinusoidal displacement curve without an external force. For the ideal displacement input $y_d(t) = [300 + 100\sin(0.314t)]$ [mm], the maximum relative synchro error was 5%. The ideal displacement input is labeled as number 3 in Figs. 14-16. Since the cylinder stroke is 600 mm, it is straightforward to choose the tracking of the sinusoidal displacement from the middle of the cylinder. The input signal frequency was based on the fact that typically pneumatic system's frequency is low. The system's response to step and sinusoidal signal and the choice of the signal's excitation frequency was based on what other researchers usually studied in analysis of single cylinder systems.

Fig. 15 shows the synchro tracking results with the 17

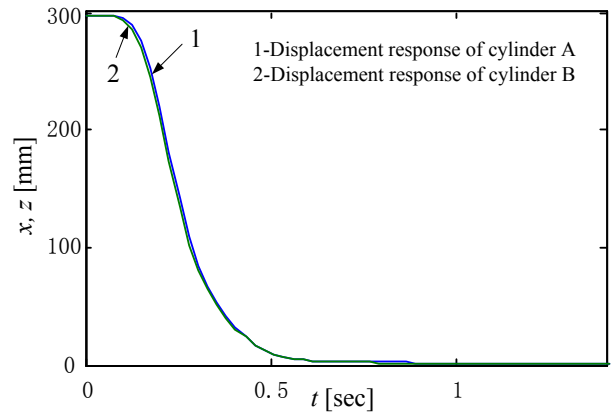


Fig. 13. The response of the synchro control without external force using the proposed control strategy.

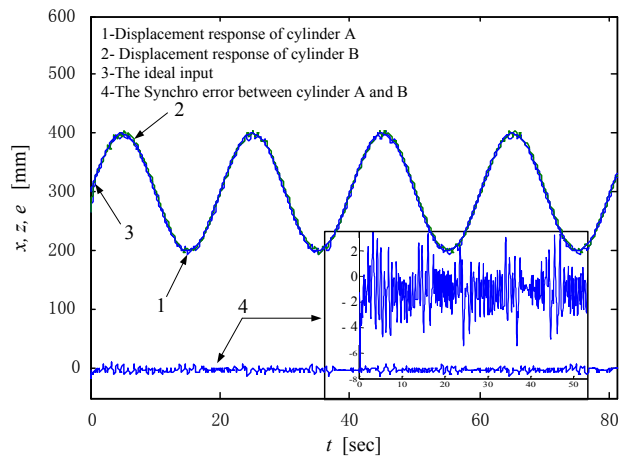


Fig. 14. Tracking of the synchro control without external force using the new control strategy.

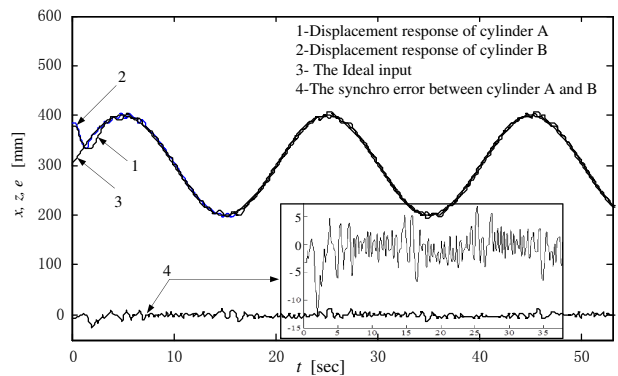


Fig. 15. Tracking of synchro control with 17 N external force.

N external force applied to cylinder A, for which the maximum relative synchro error was 5%. The results show that the control strategy possesses certain robustness to external disturbances. Fig. 16 shows the synchro tracking results with the 34 N external force applied to cylinder

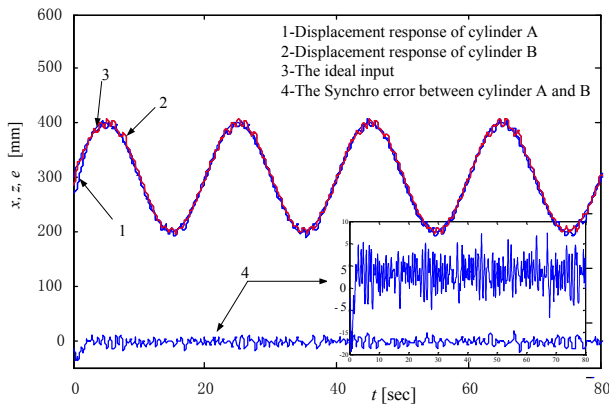


Fig. 16. The tracking of synchro control with 34 N external force.

A, for which the maximum relative synchro error was 8%. According to the experimental results, the proposed control strategy performed much better compared to the PID controller. The synchro error was reduced and the control accuracy was enhanced.

6. CONCLUSION

In this paper, the system model was developed using both theoretical and experimental methods. A synchronous position control strategy was proposed to achieve good position tracking performances in the presence of load disturbances and system uncertainties. Since electro-pneumatic systems are highly nonlinear – especially at low velocities – a bi-cylinder sliding mode controller was used to eliminate ‘chattering’ in the cylinder and improve the system robustness. Experimental results showed the controller’s insensitivity to external disturbances and ability to reduce the synchro position error. This technique can be readily applied to bi-cylinder systems by choosing suitable PID parameters for the synchro PID controllers. As condition limits, the proposed control strategy only used two cylinders with one air source. Since in many industrial applications there is only one air source for many cylinders, the nonlinearity resulting from low pressure makes the control condition more serious in terms of air compressibility and friction effects. Future work will study the performance of multi-cylinder systems with low pressure conditions.

NOMENCLATURE

A_p	- Piston area
u	- Valve input opening size
M_1	- Mass load of cylinder A
M_2	- Mass load of cylinder B
x	- Piston output displacement of cylinder A
x_1	- Piston output displacement of cylinder A

x_2	- Piston output velocity of cylinder A
$p_{x1}(x_3)$	- Left chamber pressure of the cylinder A
$p_{x2}(x_4)$	- Right chamber pressure of the cylinder A
z	- Piston output displacement of cylinder B
z_1	- Piston output displacement of cylinder B
z_2	- Piston output velocity of cylinder B
$p_{z1}(z_3)$	- Left chamber pressure of the cylinder B
$p_{z2}(z_4)$	- Right chamber pressure of the cylinder B
p_s	- Supply pressure
p_e	- Exhaust pressure
P_d	- Downstream pressure
P_u	- Upstream pressure
P_{atm}	- Atmospheric pressure
F_{f1}	- Friction force in cylinder A
F_1	- External force in cylinder A
k	- Specific heat $k = 1.4$
C_r	- Critical pressure ratio = 0.528
C_d	- Valve orifice discharge coefficient = 0.8
C_0	$= \sqrt{k \cdot \left(\frac{2}{k+1}\right)^{(k+1)/(k-1)}} = 0.685$ (constant)
V_{10}	- Initial volumes of the chamber
V_{20}	- The volumes of the long hole in the cylinder
L	- Piston stroke
R	- Gas Constant [J/kg·K]
δ	- Valve’s clearance
A_f	- Valve’s leakage measure
T	- Absolute temperature $T = 294$ K
F_{f2}	- Friction force in cylinder B
F_2	- External force in cylinder B
D	- Piston of valve’s diameter
v_d	- Velocity cut-off point
K_f	- Exact viscous friction factor
F_{kc}	- Exact Coulomb friction factor

REFERENCES

- [1] S. Scavarda, A. Lellal, and E. Richard, “Linear zed models for an electro pneumatic cylinder servovalve system,” *Proc. of the 3rd International Conference in Advanced Robotics*, pp. 13-15, 1987.
- [2] M. Sorli, G. Figliolini, and S. Pastorelli, “Dynamic model and experimental investigation of a pneumatic proportional pressure valve,” *IEEE/ASME Trans. Mechatronics*, vol. 9, pp. 78-86, 2004.
- [3] J. Wang, J. D. Wang, N. Daw, Q. H. Wu, “Identification of pneumatic cylinder friction parameters using genetic algorithms,” *IEEE/ASME Trans. Mechatronics*, vol. 9, pp. 100-107, 2004.
- [4] G. M. Bone, M. Xue, and J. Flett, “Position control of hybrid pneumatic-electric actuators using discrete-valued model-predictive control,” *Mechatronics*, vol. 25, pp. 1-10, 2015. [click]
- [5] P. Harris, S. Nolan, and G. E. O’Donnell, “Energy optimisation of pneumatic actuator systems in manufacturing,” *Journal of Cleaner Production*, vol. 72, pp. 35-45, 2014. [click]

- [6] J. Li, K. Kawashima, T. Fujita, and T. Kagawa, "Control design of a pneumatic cylinder with distributed model of pipelines," *Precision Engineering*, vol. 37, no. 4, pp. 880-887, 2013. [click]
- [7] B. S. Park and S. J. Yoo, "Adaptive leader-follower formation control of mobile robots with unknown skidding and slipping effects," *International Journal of Control, Automation and Systems*, vol. 13, no. 3, pp. 587-594, 2015. [click]
- [8] Z. Qiu, B. Wang, X. Zhang, and J. Han, "Direct adaptive fuzzy control of a translating piezoelectric flexible manipulator driven by a pneumatic rodless cylinder," *Mechanical Systems and Signal Processing*, vol. 36, no. 2, pp.290-316, 2013. [click]
- [9] J. K. Lee, Y. H. Choi, and J. B. Park, "Sliding mode tracking control of mobile robots with approach angle in cartesian coordinates," *International Journal of Control, Automation and Systems*, vol. 13, no. 3, pp. 718-724, 2015. [click]
- [10] G. M. Bone and S. Ning, "Experimental comparison of position tracking control algorithms for pneumatic cylinder actuators," *IEEE/ASME Trans. on Mechatronics*, vol. 12, pp. 557-561, 2007.
- [11] T. Nguyen, J. Leavitt, F. Jabbari, and J. E. Bobrow, "Accurate sliding-mode control of pneumatic systems using low-cost solenoid valves," *IEEE/ASME Trans. Mechatronics*, vol. 12, pp. 216-219, 2007.
- [12] B. Xu, S. Abe, and N. Sakagami, "Robust nonlinear controller for underwater vehicle-manipulator system," *Proc. of the IEEE/ASME International Conference on Advanced Intelligent Mechatronics*, pp. 711-716, 2005.
- [13] M. Taghizadeh, A. Ghaffari, and F. Najafi, "Improving dynamic performances of PWM-driven servo-pneumatic systems via a novel pneumatic Circuit," *ISA Transactions*, vol. 48, no. 4, pp. 512-518, 2009.
- [14] S. Sivrioglu and K. Nonami, "Sliding mode control with time-varying hyper plane for AMB systems," *IEEE/ASME Trans. Mechatronics*, vol. 3, no. 1, pp. 51-59, 1998.
- [15] L. Fridman, "Singularity perturbed analysis of chattering in relay control systems," *IEEE Trans. on Automatic Control*, vol. 47, pp. 2079-2084, 2002.
- [16] G. Bartolini, A. Ferrara, and E. Usai, "Chattering avoidance by second order sliding-mode control," *IEEE Trans. on Automatic Control*, vol. 43, pp. 241-246, Feb. 1998.
- [17] A. C. Huang and Y.C. Chen, "Adaptive multiple-surface sliding control for non-autonomous systems with mismatched uncertainties," *Automatica*, vol. 40, no. 11, pp. 1939-1945, 2008. [click]
- [18] S. Khoo, Z. Man, and S. Zhao, "Comments on adaptive multiple-surface sliding control for non-autonomous systems with mismatched uncertainties," *Automatica*, vol. 44, pp. 2995-2998, 2008. [click]
- [19] Y. Orlov, L. Aguilar, and J. C. Cadiou, "Switched chattering control vs. backlash/friction phenomena in electrical servo-motors," *Int. J. Control*, vol. 76, no. 9, pp. 959-967, 2003. [click]
- [20] I. Boiko, L. Fridman, and M. I. Castellanos, "Analysis of second-order sliding-mode algorithms in the frequency domain," *IEEE Transactions on Automatic Control*, vol. 49, no. 6, pp. 946-950, 2004.
- [21] K. Sato and Y. Sano, "Practical and intuitive controller design method for precision positioning of a pneumatic cylinder actuator stage," *Precision Engineering*, vol. 38, no. 4, pp. 703-710, 2014. [click]
- [22] V. Yuriy, V. P. Yuriy, and A. A. Sergey, "Computer simulation of electro-pneumatic drives for vertical motion mobile robots," *Procedia Engineering*, vol. 100, pp. 1003-1012, 2015. [click]
- [23] F. Abry, X. Brun, M. Di Loreto, S. Sesmat, and É. Bideaux, "Piston position estimation for an electro-pneumatic actuator at standstill," *Control Engineering Practice*, vol. 41, pp. 176-185, 2015. [click]
- [24] National Instruments; Available: <http://www.ni.com/lwcvl/>
- [25] B. Armstrong-Helouvry, *Control of Machines with Friction*, Kluwer Academic, Boston, 1991.



Hong Zhao received her Ph.D. degree from Xi'an Jiaotong University, Xi'an, Shannxi Province, China in 2003. She is currently an Associate Professor in China University of Petroleum (Beijing). Her research interests include mechanical and electrical transmission control, virtual instrument measurement and control technology.



Pinhas Ben-Tzvi received his B.S. degree (*summa cum laude*) in mechanical engineering from the Technion-Israel Institute of Technology, Israel and his M.S. and Ph.D. degrees in mechanical engineering from the University of Toronto, Canada. He is currently an Associate Professor of Mechanical Engineering and Electrical and Computer Engineering, and the found-

ing Director of the Robotics and Mechatronics Laboratory at Virginia Tech. His current research interests include robotics and intelligent autonomous systems, human-robot interactions, mechatronics, mechanism design and system integration, dynamic systems and control, and novel sensing and actuation. Application areas are varied and range from search & rescue on rough terrain to medical diagnostics, surgery, and therapy. Dr. Ben-Tzvi is a senior member of IEEE and a member of ASME.